ELSEVIER

Journal of the Mechanics and Physics of Solids
51 (2003) 2259–2280

JOURNAL OF THE
MECHANICS AND
PHYSICS OF SOLIDS

www.elsevier.com/locate/jmps

Mechanics of the human red blood cell deformed by optical tweezers☆

M. Dao[a], C.T. Lim[b], S. Suresh[a,c,*]

[a] *Department of Materials Science and Engineering, Massachusetts Institute of Technology, 77 Massachusetts Avenue, Cambridge, MA 02139, USA*

[b] *Division of Bioengineering and Department of Mechanical Engineering, The National University of Singapore, 9 Engineering Drive 1, Singapore 117576, Singapore*

[c] *Department of Mechanical Engineering, Massachusetts Institute of Technology, 77 Massachusetts Avenue, Cambridge, MA 02139, USA*

Abstract

The mechanical deformation characteristics of living cells are known to influence strongly their chemical and biological functions and the onset, progression and consequences of a number of human diseases. The mechanics of the human red blood cell (erythrocyte) subjected to large deformation by optical tweezers forms the subject of this paper. Video photography of the cell deformed in a phosphate buffered saline solution at room temperature during the imposition of controlled stretching forces, in the tens to several hundreds picoNewton range, is used to assess experimentally the deformation characteristics. The mechanical responses of the cell during loading and upon release of the optical force are then analysed to extract the elastic properties of the cell membrane by recourse to several different constitutive formulations of the elastic and viscoelastic behavior within the framework of a fully three-dimensional finite element analysis. A parametric study of various geometric, loading and structural factors is also undertaken in order to develop quantitative models for the mechanics of deformation by means of optical tweezers. The outcome of the experimental and computational analyses is then compared with the information available on the mechanical response of the red blood cell from other independent experimental techniques. Potential applications of the optical tweezers method described in this paper to the study of mechanical deformation of living cells under different stress states and in response to the progression of some diseases are also highlighted.

Keywords: Human red blood cell membrane; Large deformation; Optical tweezers; Shear modulus; Bending stiffness; Hyperelasticity; Computational model

☆ Video clips (see movies 1–3) of the optical trap experiments on the red blood cell showing large deformation and video clips of three-dimensional computational simulations of the biconcave cell membranes subjected to large deformation can be viewed at the supplementary material available along with the electronic archive of this paper.

* Corresponding author. Tel.: 617-253-3320; fax: 617-253-0868.
E-mail address: ssuresh@mit.edu (S. Suresh).

0022-5096/$ - see front matter © 2003 Elsevier Ltd. All rights reserved.
doi:10.1016/j.jmps.2003.09.019

1. Introduction

The deformation of human red blood cell (erythrocyte) has long been a topic of considerable scientific interest and real-life significance (see, for example, Evans and Skalak, 1980; Fung, 1993; Boal, 2002). The human red blood cell with a biconcave shape and an average diameter of about 8 μm has a typical life span of 120 days during which time it circulates through the human body nearly half a million times. During the course of its circulation, it undergoes severe elastic deformation as it passes through narrow capillaries whose inner diameter is as small as 3 μm. The 'biconcave' shape of the red blood cell is transformed into a 'bullet' shape during blood flow through small capillaries, and the cell recovers fully to its original shape when the constraint or loading causing the shape change is released.

Studies of the deformation characteristics of the human red blood cell and its membrane have been of interest in the biomechanics literature for several reasons.

(1) The red blood cell has a relatively simple structure in that its membrane comprising the phospholipid bilayer with the intervening hydrophobic molecular network contains a fluid (cytosol) of fixed volume and known viscosity. The red blood cell does not contain a nucleus. Consequently, it has often been regarded as a "model system" in the study of single living cells. In light of these considerations, the mammalian red blood cell constitutes a convenient system for fundamental studies of how cell membranes convert mechanical forces into biological responses, and how structural, chemical and biological signals and changes in the cell affect the manner in which cell membranes detect, produce or support mechanical forces (e.g., Bao and Suresh, 2003).
(2) The simple, axisymmetric, biconcave shape of the red blood cell is relatively more amenable to the development of detailed theoretical/computational models than other cells of more complex geometry. Early studies of cell mechanics have mostly visualized the red cell as a thin elastic membrane which surrounds a viscous fluid (e.g., Hochmuth et al., 1979).
(3) The rounded disc shape of the red blood cell readily facilitates single cell mechanical deformation experiments such as those involving micropipette aspiration or optical tweezers (see later discussion).
(4) Blood flow in microcirculation is influenced significantly by the deformability of the red blood cell which, in turn, is determined by such mechanical and geometrical factors as the surface area, elasticity and viscosity of the cell membrane and the volume and viscosity of the cytosol.
(5) There is a direct connection between the progression of certain inherited diseases and the mechanical deformation characteristics of the red blood cell. Consider the case of sickle cell disease which is caused by a defect in the haemoglobin structure as a result of the substitution of thymine for adenine in the β-globin gene, and the attendant encoding of valine instead of glutamic acid in the sixth position of the haemoglobin β-chain (Platt, 1995). As a consequence of this abnormality haemoglobin, which transports oxygen to the organs and tissues in the body, clusters episodically. The shape of the red cell is altered and its deformability and

biorheology (ability to be transported through the blood vessels normally) are adversely affected. This can result in severe pain as the tissues surrounding the blood vessels receive insufficient oxygen.

(6) It is now realized that the red blood cell can serve as the site for the maturation of intracellular parasites which can lead to the progression of fatal diseases by affecting the mechanical deformation and functional properties of the cell itself. Consider the case of malaria, the most widespread parasitic disease of humans that claims the lives of some 2–3 million people annually. This disease is caused by the protozoa of the genus *Plasmodium Falciparum* (see, for a review, Cooke et al., 2001). The structure of the cell cytoplasm, the shape of the cell and the molecular constitution of its membrane are altered during the maturation of the parasite in the cell so that red blood cell progressively loses its ability to undergo large deformation (Glenister et al., 2002; Lim et al., 2003); furthermore, the adhesiveness of the red cell with other cells, such as the vascular endothelium, is also increased (Cooke et al., 2001). Interestingly, patients with sickle cell disease exhibit resistance to malaria.

Characterization of deformation of red blood cell has been achieved through a variety of experimental techniques. Most common among these methods is the micropipette aspiration technique (Evans, 1973; Hochmuth et al., 1973; Hochmuth and Waugh, 1987), in which the stepwise increase of a suction pressure causes the cell to be drawn into a glass tube, whose inner diameter, in conjunction with the aspiration pressure, can be appropriately chosen so as to control the extent of deformation. The pressure is held over a certain duration during which the deformation of the cell is recorded by means of optical microscopy. The method can also be used, under appropriate conditions, to assess the viscoelastic relaxation characteristics of the cell upon release of the aspiration pressure. By matching the experimentally observed geometry changes of the whole cell for given loading and configurational parameters of the experiment with theoretically predicated responses, the elastic modulus, viscosity and characteristic time for relaxation of the cell membrane can be extracted from such experiments (Evans and Skalak, 1980). With recent advances in micromechanical and nanomechanical characterization tools which can monitor/impose force and displacement to a resolution on the order of picoNewton (10^{-12} N) and nm (10^{-9} m), respectively, there is a constant search for additional experimental tools which can provide further insights into the mechanical deformation characteristics of living cells (see Van Vliet et al., 2003, for a comprehensive review). In particular, there is a continual need to develop new experimental methods that are capable of imposing widely differing stress states on living cells in a controlled mode and with high precision, so that the multiaxial deformation characteristics of single cells and membranes in a fluid environment can be accurately captured.

Development of experimental techniques based on optical or laser traps (also commonly referred to as optical or laser tweezers) has facilitated mechanical deformation of whole biological cells at forces ranging from tens to hundreds of pN. This technique is predicated on the phenomenon that upon passing through a high-refractive-index dielectric object, the photons from the laser beam undergo a change in momentum which

then exerts a force on the object and pushes it towards the focal point of the laser beam. This results in the object being "trapped" by the laser beam. For example, a dielectric bead of silica when so trapped by a laser beam can be physically moved as the laser beam is displaced. If such a bead is attached strongly to the surface of a cell, it serves as a handle or grip and displaces the cell membrane. The physics of optical traps is described in detail elsewhere (Sheetz, 1998). The optical tweezers method can be used to stretch the cell directly in one or more directions by trapping beads that are strategically attached to the cell surface through specific or non-specific binding. Human red blood cells have been stretched directly using optical traps to maximum forces of 60 pN by recourse to two or three bead attachments on cell surfaces (Hénon et al., 1999; Sleep et al., 1999; Lenormand et al., 2001). Such forces, however, are insufficient to induce large diameter changes in the human red blood cell which is representative of the extent of large deformation commonly encountered in vivo. These initial studies did not capture the complete deformation characteristics of the cell by continuously monitoring the changes in axial and transverse diameters during loading and unloading of the cell. In order to overcome these restrictions, the present study and the parallel effort of Lim et al. (2004) have sought to refine and extend the optical tweezers method for the study of large deformation of single biological cells, by providing the following innovations: (a) direct stretching of the cell to optical forces as large as 600 pN, nearly an order of magnitude larger than that achieved previously for stretching the blood cell, (b) the use of larger bead sizes so that any possibility of the heating of the cell by laser light is completely avoided, and (c) use of a fully three-dimensional computational model of cell deformation, with the cytosol included inside the cell membrane, to extract key elastic and viscoelastic properties of the cell membrane from the optical tweezer experiments.

Drawing on the parallel work of Lim et al. (2004), this paper provides a detailed discussion of the mechanics of large deformation of the human red blood cell by recourse to computational simulations. In particular, systematic parametric analysis of the effects of cell membrane shear and bending rigidity, the cell interior volume, the variations in cell diameter, the conditions of contact between the cell membrane and the beads trapped by the laser on the large deformation characteristics of the cell are addressed in this paper with a view to elucidate the mechanics of optical tweezers experiments for the study of living cells. The present computational simulations are also carried out in the context of a variety of available constitutive descriptions of the cell membrane. The implications of the predictions are assessed in light of the optical tweezers experiments and in comparisons with results obtained from other techniques, such as micropipette aspiration, wherever appropriate.

2. Background on experimental methods

The experimental set up used to impose large deformation on the human red blood cell using optical tweezers is schematically sketched in Fig. 1. The key component of this set up is a 1.5 W diode pumped Nd:YAG laser source (Cell Robotics, Albuquerque, NM) connected to an inverted microscope (Leica Microsystems,

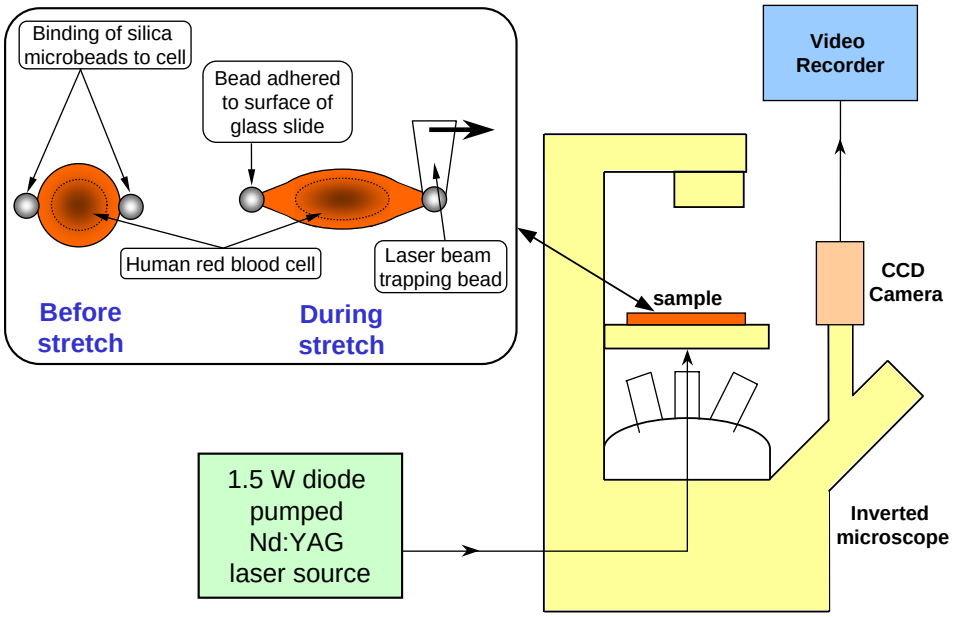

Fig. 1. Illustration of the optical trap setup which comprises the laser source, the inverted microscope, a CCD camera and a video recorder. The sample consists of two silica microbeads, 4.12 μm in diameter non-specifically binded to the red cell at diametrically opposite points. The left bead is anchored to the surface of the glass slide. The right bead can be trapped using the laser beam and stretching force applied to it via the movement of the laser beam.

Wetzlar, Germany). The laser beam is used to trap a high-refractive-index silica bead which is attached to the cell surface. The 1.5 W laser beam when used with silica microbeads of 4.12 μm in diameter can generate large forces that are nearly an order of magnitude higher than those used for deforming red blood cells in previous studies (Hénon et al., 1999; Sleep et al., 1999; Parker and Winlove, 1999). Two silica microbeads, which act as handles, are attached diametrically across the cell through non-specific binding as shown in Fig. 1. As the present optical tweezers system is designed to consist only of a single optical trap, one of the microbeads is adhered to the glass surface while the other is free to be trapped using the laser beam. By moving one of the beads with the laser beam, the cell is directly stretched. The trapping force exerted on the microbead can be changed, up to a maximum value of about 600 pN, by varying the laser power setting. Thereafter, changes in axial (in the direction of stretch) and transverse (normal to that of stretch) diameters are recorded using a CCD camera and video recorder. The red blood cell, placed in a phosphate buffered saline solution, was stretched by optical tweezers in the room temperature laboratory environment. Further details of sample preparation, force calibration, experimental set up and data collection can be found in Lim et al. (2004).

3. Theoretical background and computational model

3.1. Constitutive response

As illustrated in Fig. 2(a), the human red blood cell membrane comprises the phospholipid bilayer, the underlying spectrin network and transmembrane proteins. The (composite) cell membrane structure is commonly modelled as an incompressible effective continuum, Fig. 2(b). Evans (1973) suggested that the relationship between the membrane shear stress T_s (in units of force per unit length) and deformation is of the form:

$$T_s = 2\mu\gamma_s = \frac{\mu}{2}(\lambda_1^2 - \lambda_2^2), \tag{1a}$$

$$T_s = \frac{1}{2}(T_1 - T_2) \quad \text{and} \quad \gamma_s \equiv \frac{1}{2}(\varepsilon_1 - \varepsilon_2) = \frac{1}{4}(\lambda_1^2 - \lambda_2^2), \tag{1b}$$

$$\lambda_1\lambda_2 = 1, \tag{1c}$$

where T_1 and T_2 are the in-plane principal membrane stresses, ε_1 and ε_2 are the in-plane principal Green's strains of the membrane, λ_1 and λ_2 are the principal stretch ratios, μ is the membrane shear modulus (assumed to be constant and expressed in units of force per unit length) and γ_s is the shear strain. Note that Eq. (1c) reflects the assumption that the total membrane area is constant during deformation. For the case

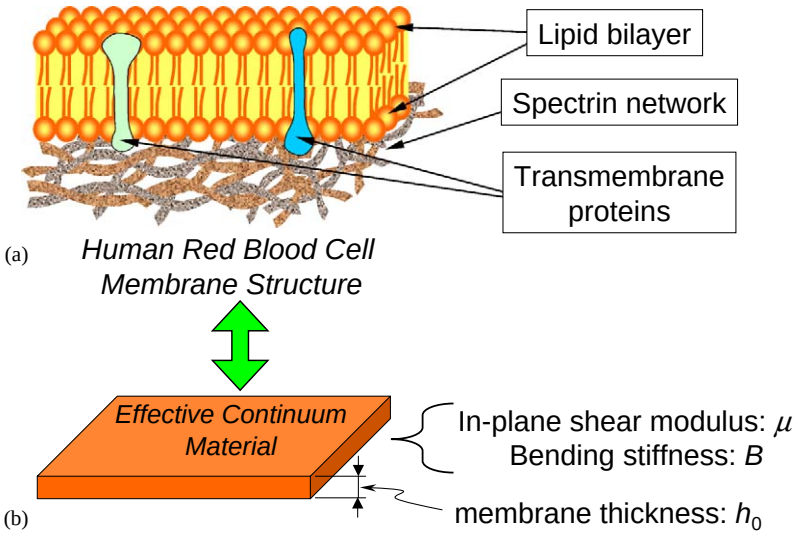

Fig. 2. Illustration of the effective continuum shell model. (a) The human red blood cell membrane structure comprises the lipid bilayer, the spectrin network and transmembrane proteins. (b) The (composite) cell membrane structure is modelled using a hyperelastic effective continuum material.

of uniform deformation, the ratios of the current diameter to the initial diameter in the axial and transverse directions of the cell correspond approximately to the stretch ratios λ_1 and λ_2, respectively. However, for the experiments using the micropipette aspiration and optical trap techniques, the deformation is nonuniform. The constitutive model described in Eq. (1) has been used for interpreting the mechanical response of the red blood cell in numerous experimental studies conducted using the micropipette aspiration technique (Evans, 1973; Evans and Skalak, 1980).

Large deformation response of the red blood cell has also been analyzed using other variations of such continuum constitutive models. One such approach is predicated on use of a hyperelastic effective material model (Lim et al., 2004). The simplest first order formulation in this case is the incompressible (constant volume) neo-Hookean form where the strain energy potential function (Simo and Pister, 1984) is given by

$$U = \frac{G_0}{2}(\lambda_1^2 + \lambda_2^2 + \lambda_3^2 - 3), \tag{2}$$

where G_0 is the initial bulk shear modulus, and λ_i $(i=1,2,3)$ are the principal stretches. If the membrane is assumed to be incompressible, $\lambda_1\lambda_2\lambda_3 = 1$. The potential function in Eq. (2) defines the nonlinear elastic stress–strain behavior. The neo-Hookean hyperelastic potential is known to be reasonably accurate when the maximum strain is on the order of 100%. For a hyperelastic thin membrane subjected to uniaxial stretch $(T_2 = 0)$, the uniaxial membrane stress T_1 can be derived from Eq. (2),

$$T_1 = h\frac{\partial U}{\partial \lambda_1} = G_0 h_0(\lambda_1^{1.5} - \lambda_1^{-1.5}), \tag{3}$$

where h is the current membrane thickness, and h_0 is the initial membrane thickness. Therefore, under uniaxial stretch the membrane shear stress is

$$T_s = \frac{1}{2}(T_1 - T_2) = \frac{G_0 h_0}{2}(\lambda_1^{1.5} - \lambda_1^{-1.5}) \tag{4}$$

and the (instantaneous) membrane shear modulus μ is given as

$$\mu(\lambda_1) = \frac{1}{2}\frac{\partial T_s}{\partial \gamma_s} = \frac{3G_0 h_0(\lambda_1^{0.5} + \lambda_1^{-2.5})}{4(\lambda_1 + \lambda_1^{-3})}. \tag{5}$$

From Eq. (5), the initial in-plane membrane shear modulus is found to be $\mu_0 = 0.75 G_0 h_0$. Fig. 3(a) schematically shows the shear stress versus shear strain response of such a neo-Hookean hyperelastic material during uniaxial stretch. The membrane shear modulus typically decreases from its initially high value, μ_0, to a relatively smaller value, μ_l, at larger strains, before attaining a higher value, μ_f, again prior to final failure. The slope of the membrane shear stress (T_s) versus shear strain ($2\gamma_s$) is therefore a decreasing function of shear strain from the initial to the intermediate region, as shown in Fig. 2(b). For the simple first order neo-Hookean material formulated in Eq. (2), only the first stage (μ_0) and the second stage (μ_l) are present. Specifically, μ_l is taken here at a relatively large stretch ratio of $\lambda_1 = 3$ under uniaxial tension. As shown later, the strain values introduced in the cell membrane during large deformation in the present optical trap experiments correspond to the intermediate region of the stress–strain curve in

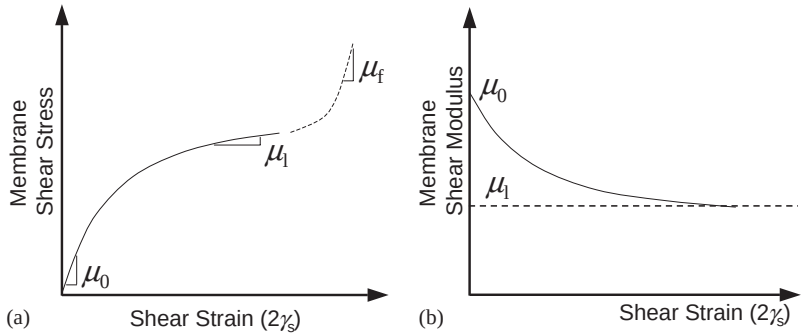

Fig. 3. Schematic illustration of the hyperelastic constitutive response used in some of the computational simulations. (a) Uniaxial stress–strain response. (b) The variation of the membrane shear modulus with the progression of deformation in the early region and in the in-between region, where strains are representative of the large deformation response achieved in the present optical tweezer experiments. The final deformation regime with the shear modulus of μ_f is not shown in this figure.

Fig. 3(a) where the membrane shear modulus is close to μ_1. Therefore, the present analysis does not include the deformation response indicated by the dashed line in Fig. 3(a) (i.e., that corresponding to the final shear modulus, μ_f). When the constant membrane area constraint, i.e. the condition that $\lambda_1\lambda_2 = 1$ (with the third principal stretch, $\lambda_3 = 1$) is enforced in Eq. (2), the constitutive description of Eq. (2) becomes equivalent to that of Eq. (1), where the in-plane membrane shear modulus stays at a constant value of $\mu = G_0 h_0$ throughout the entire deformation history.

For a thin shell structure, the key parameters of interest in the characterization of large deformation are the in-plane shear modulus μ and the bending modulus B. For the accepted range of literature values of $B_0 = 1.7 \times 10^{-19}$–$7 \times 10^{-19}$ N m for the human red blood cell (Evans, 1983; Sleep et al., 1999), our simulations indicate that the force required to produce a given stretch ratio in the axial or transverse direction varied by less than 5%, when stretching force was larger than 50 pN. Therefore, only the results obtained using a typical value of $B_0 = 2 \times 10^{-19}$ N m are presented here. In conducting the parameter studies, the initial shear modulus value μ_0 can be chosen first. This subsequently determines the uniaxial large strain membrane shear modulus μ_1. By incrementally varying the values of μ_0 (as well as μ_1), the closest fit to the experimental axial and transverse diameters during large deformation stretch determines the estimated membrane shear modulus value.

The cytosol is assumed to be a fluid which acts to preserve the interior volume (V_0) of the red blood cell during deformation as well as to maintain the even distribution of the internal (hydraulic) fluid pressure (p) on the inner membrane surface, i.e.

$$V(t) = V_0 \quad \text{and} \quad p_e(t) = p(t), \tag{6}$$

where $V(t)$ is the current cell interior volume and $p_e(t)$ is the normal pressure acting on the internal surface of each shell element (cell membrane) of the finite element mesh at any instantaneous time t. The viscous energy dissipation of the cytoplasm

within the red cell filled with concentrated haemoglobin solution is known to be two orders of magnitude smaller than that of the membrane (Evans and Hochmuth, 1976). The viscosity of the cytosol can therefore be ignored. In order to explore possible effects of cell membrane permeability, companion computations without cytosol were also carried out in the present work.

3.2. Computational model

Evans and Fung (1972) estimated the shape of human red blood cells and an average biconcave shape function was given as

$$Z = \pm 0.5R_0 \left[1 - \frac{X^2 + Y^2}{R_0^2}\right]^{\frac{1}{2}} \left[C_0 + C_1 \frac{X^2 + Y^2}{R_0^2} + C_2 \left(\frac{X^2 + Y^2}{R_0^2}\right)^2\right], \tag{7a}$$

$$R_0 = 3.91\ \mu\text{m}, \quad C_0 = 0.207161, \quad C_1 = 2.002558, \quad \text{and}$$
$$C_2 = -1.122762, \tag{7b}$$

where $2R_0$ is the average cell diameter in the axial direction. Different initial cell diameter values ranging from 7 to 8.5 μm in Eq. (7) can be explored to investigate the effect of cell size variations. Fig. 4(a) shows the original equilibrium shape of the three-dimensional biconcave model of the red blood cell constructed using the dimensions specified in Eq. (7). The stretching force is applied to the silica microbeads which are attached diametrically at opposite ends of the cell. The silica beads are modelled as rigid spheres and are assumed to be attached to the cell over a small oval region with a diameter of between 1 and 2 μm so that the final contact conditions could be properly simulated. Because of symmetry, it suffices to model only half of the red blood cell. Fig. 4(b) shows the original mesh of the biconcave model which contains 12,000 three-dimensional shell elements. Four-noded, bilinear, reduced integration shell elements are used. The simulations have been performed using the commercially available general purpose finite element package, ABAQUS (ABAQUS, 2002). Fig. 4(c) shows an axisymmetric spherical shell model which was used for some simulations in an attempt to develop a basis for comparison with the results derived from the more realistic biconcave cell model. Another reason for performing additional simulations with the spherical shell model is that some recent studies (Parker and Winlove, 1999) on small deformation of red cells using optical traps invoked analysis of spherical geometry in the interpretation of experiments. Thus, the trends extracted from the present work could be systematically compared with prior studies. Similar to the case of the biconcave model, the silica beads are assumed to be attached to the spherical cell over a small circular region with diameter between 1 and 2 μm. Computations using the red cell model with and without the cytosol were performed. All the results presented below in the parametric studies pertain to conditions where the cytosol is included in the computational simulations, unless specified otherwise.

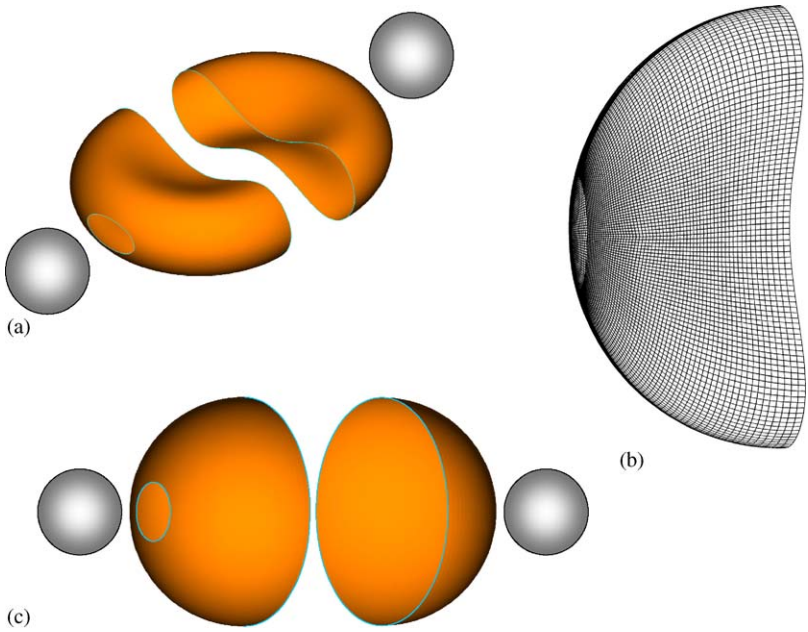

Fig. 4. Finite element model setup of the three-dimensional geometry of the human red blood cell. (a) Original shape of the three dimensional biconcave model. The rigid silica beads were assumed to be attached to the cell over a small oval region with a diameter between 1 and 2 μm. Only half of the red blood cell was modelled because of symmetry. (b) Original mesh design of the biconcave model, where 12,000 three-dimensional shell elements were used in the simulations. (c) Companion axisymmetric spherical model. The silica beads were assumed to be attached to the cell over a small circular region with a diameter between 1 and 2 μm. The cytosol can be effectively modelled as a hydraulic fluid.

4. Results

Fig. 5(a) shows a sequence of optical images revealing large deformation response of a red cell at different stretching forces. At stretch force of 340 pN, the axial diameter of the cell increased by 50% and the transverse diameter was reduced by more than 40%. Fig. 5(b) is a plot of the computational results of the plane view of the cell at different values of imposed stretching forces. The presence of a volume-preserving fluid inside the cell was assumed in these simulations, following the approximations outlined in the previous section. Fig. 5(b) also contains contours of constant maximum principal strain on the cell membrane. Note that, as anticipated, regions of cell membrane in physical contact with the silica beads undergo the maximum strain, which is as much as 100 –120% at the maximum force of 340 pN indicated in the figure. With the initial value of the membrane shear modulus taken to be $\mu_0 = 22.5$ μN/m, and with the contact diameter d_c between the bead and cell fixed at 2 μm, the value of membrane shear modulus μ_l in the intermediate stage of large deformation which led to quantitative agreement, in axial and transverse diameters at different force levels, between the simulation and experiment was found to be 13.3 μN/m. Fig. 5(c) shows the deformation

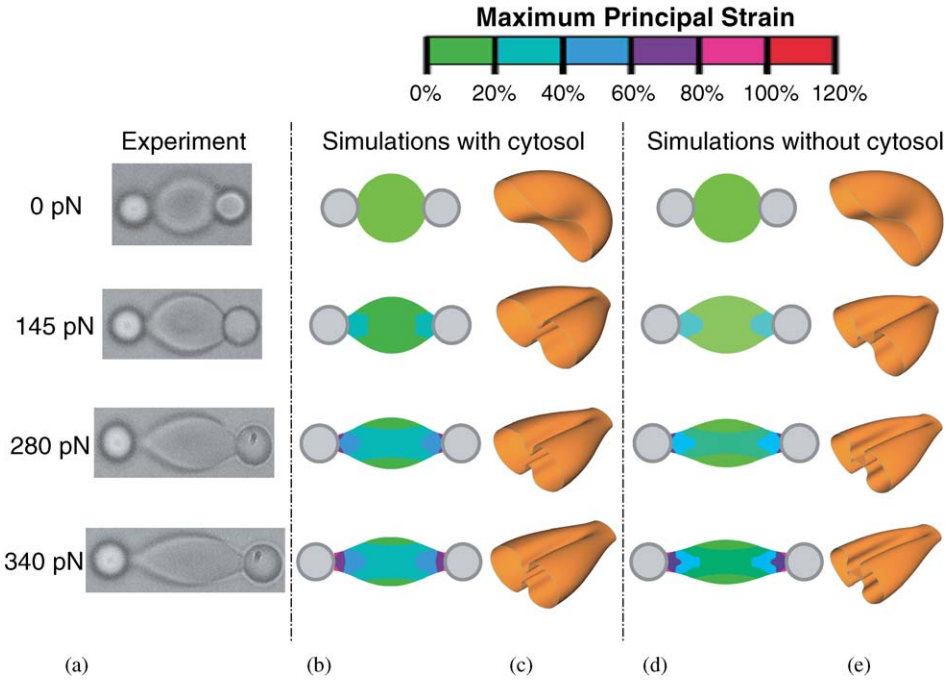

Fig. 5. Large deformation of the stretched red blood cell loaded from 0 to 340 pN. (a) Experimental observations. (b) Computed contour maps (plan view) of the constant maximum principal strain distribution (simulations with cytosol). (c) One half of the full three-dimensional biconcave shape of the erythrocyte at different loading forces (with cytosol). (d) Computed contour maps (plan view) of the constant maximum principal strain distribution (simulations without cytosol). (e) One half of the full three-dimensional biconcave shape of the erythrocyte at different loading forces (without cytosol). All simulations were performed with $\mu_0 = 22.5$ μN/m (the corresponding $\mu_1 = 13.3$ μN/m).

of the three-dimensional biconcave shape (half model view) in response to different loading forces. It is clear from this figure that the cell geometry accommodates large deformation during unidirectional stretch by the folding of the membrane. The single camera view used to record the experimental images did not facilitate clear documentation of such folding during the optical trap experiment. However, the existence of a shaded region in the interior of the cell during large deformation stretching experiments (which can be viewed in the video images posted in the supplementary material available electronically along with this paper) appears to suggest possible occurrence of such folding.

4.1. Parametric analyses

Figs. 5(d) and (e) show computational results of the corresponding plan view and half-cell three-dimensional view of the cell deformed at different forces by invoking the rather hypothetical assumption that the cell interior does not contain any fluid.

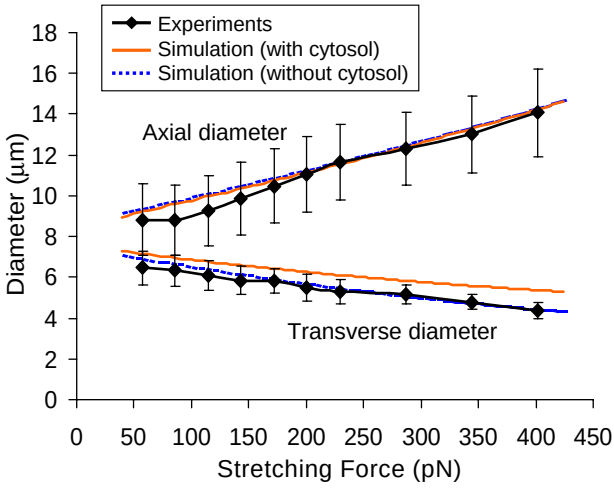

Fig. 6. Experimental and computational force versus displacement curves. The black line with error bar is the experimental observation. The solid and dashed lines are the computational predictions of the cell diameters using an in-plane shear modulus of $\mu_1 = 13.3$ μN/m (with $\mu_0 = 22.5$ μN/m), simulated with and without cytosol, respectively. Both the axial and transverse diameters are computed. The cytosol is seen having limited effect on the mechanical properties of the cell structure under large deformation uniaxial stretch, especially along the axial direction.

The absence of the cytosol is found to affect only slightly the axial and transverse diameters of the cell at different force levels. However, Fig. 5(e) suggests that without the cytosol, the centre of the biconcave disk "caves in", with the top membrane touching the bottom at higher stretching forces. This is not the case for the model with cytosol as shown in Fig. 5(c) where there is never any contact between different parts of the cell membrane. The results of computer simulations of the optical tweezer experiments thus illustrate how the cytosol serves to maintain the internal cell volume and precludes contact between different parts of the cell.

A quantitative comparison of predicted and measured changes in axial and transverse diameters of the red cell is provided in Fig. 6 for simulations with and without cytosol. This figure also shows the experimentally measured changes in axial and transverse diameters of the red cell at different stretching forces, along with the typical scatter in experimental data estimated from at least eight different experiments for each load. The responses observed for the change in axial diameters for models with or without cytosol were very close. However, for changes in the transverse diameter, the response was stiffer for the model with cytosol. The results indicate that for uniaxial direct stretch experiments, the incompressible cytosol contributes little to the axial deformability of the cell but has an important effect for deformation in the transverse direction.

In order to explore, in a parametric manner, the effect of varying the membrane shear modulus on cell deformation with optical tweezers, additional simulations were performed with two different initial values of μ_0: 18.8 and 30 μN/m. For these two cases, the membrane shear modulus μ_1 in the large deformation range in Fig. 3 was

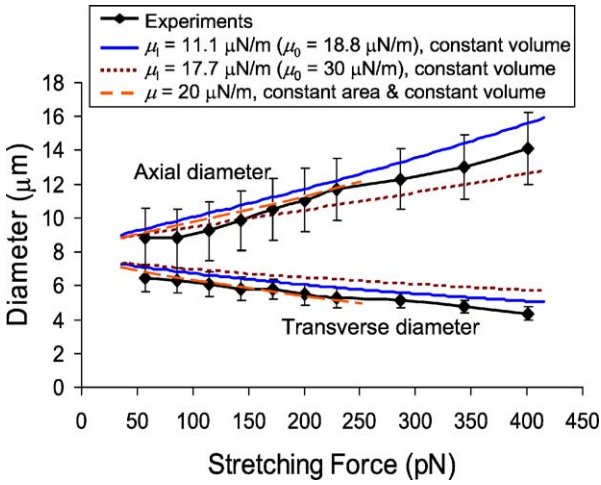

Fig. 7. Variation of measured axial and transverse diameter (solid line with scatter band) of red cell against stretching force of optical tweezers during large deformation. The solid and dotted lines represent computational predictions for the axial/transverse diameter with $\mu_l = 11.1$ and 17.7 μN/m (the corresponding $\mu_0 = 18.8$ and 30 μN/m), respectively, invoking the hyperelastic constitutive response, Eq. (2), and assuming constant cell interior volume. The computational model uses the three-dimensional biconcave disk with a contact diameter of 2 μm. Also shown are the predictions of simulations assuming both constant membrane area and constant cell interior volume, represented by long dashed lines, using the model given by Eq. (1).

chosen such that the experimental trends of changes in axial and transverse diameters as functions of the variations in stretching force were both matched by computational predictions. The resulting values of μ_l were found to be 11.1 and 17.7 μN/m, respectively, for $\mu_0 = 18.8$ and 30 μN/m. The contact size d_c was again taken to be 2 μm. Comparisons of predicted and measured changes in axial and transverse diameters of the cell are plotted in Fig. 7. Simulations performed using μ_l of 11.1 and 17.7 μN/m were able to encompass the experimental trends reasonably well over the full range of large deformation, but less so for axial diameter at small deformations.

The in-plane shear modulus range, $\mu_l = 11.1$–17.7 μN/m, estimated from our analysis using the constitutive description of Eq. (2) for large deformation with optical tweezers compares with the range of 6–10 μN/m estimated previously from micropipette aspiration experiments (Evans and Skalak, 1980; Fung, 1993). Alternatively, if we invoke the constitutive response given in Eq. (1) with constant area for the cell membrane in our three-dimensional computational simulation, the present optical tweezers experimental data can be matched by the choice of a fixed value of the membrane shear modulus, $\mu_0 = \mu_l = \mu_f = 20$ μN/m over most of the variations in axial and transverse diameter of the cell with the applied force (see Fig. 7). It should be considered that the stress state, loading mode and experimental artefacts (e.g., friction between the cell membrane and the micropipette walls in the aspiration experiments versus the contact loading at the opposite ends of the cell in the tweezers method) are very different in the two cases. It is also interesting to note that Sleep et al. (1999) reported shear modulus values

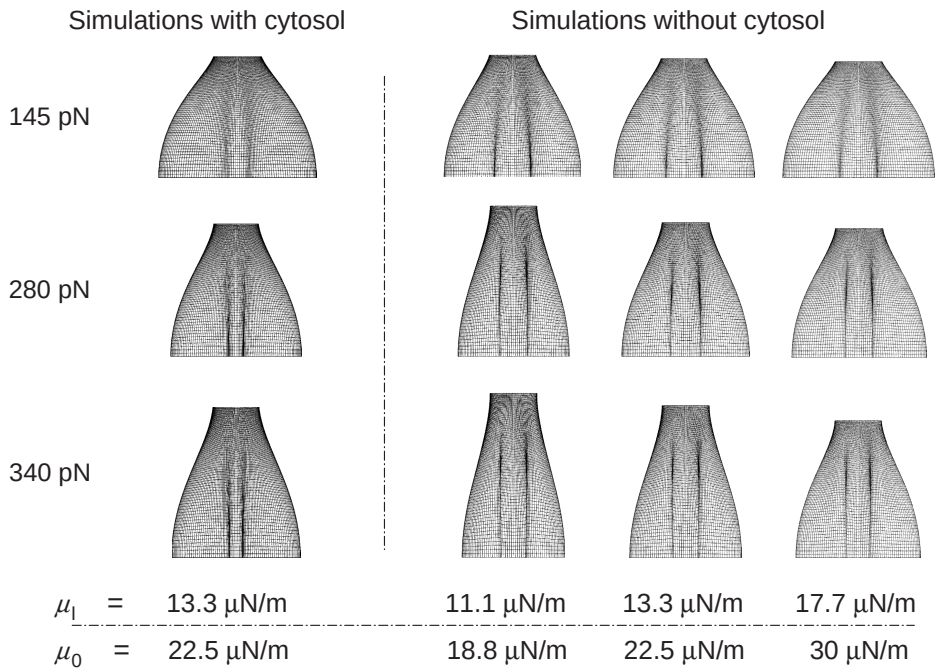

Fig. 8. Deformed meshes of the biconcave red cell model loaded from 0 to 340 pN. These deformed meshes (half model top view) are computed using in-plane shear modulus $\mu_l = 11.1$, 13.3 and 17.7 μN/m (with corresponding $\mu_0 = 18.8$, 22.5 and 30 μN/m), respectively. The red cell's structural rigidity is seen quite sensitive to variations in in-plane shear modulus of the membrane.

of up to 200 μN/m for the human red blood cell stretched by two trapped beads in an optical trap setup at a maximum force of 15 pN. They rationalize this apparent discrepancy by postulating that the membrane shear modulus from micropipette aspiration is lower than their results possibly due to the phase separation at the membrane. Additional factors could include the failure of the integral membrane proteins to follow the membrane flow during entry to capillary (Discher and Mohandas, 1996).

Fig. 8 illustrates the effects of membrane shear modulus on the configurational changes induced on the cell surface during stretching with optical tweezers. This figure shows the top view of the deformed meshes of the biconcave red cell model when subjected to stretching forces of 145, 280 and 340 pN computed using in-plane shear modulus of $\mu_l = 11.1$, 13.3 and 17.7 μN/m (with corresponding $\mu_0 = 18.8$, 22.5 and 30 μN/m), respectively, for the case without the cytosol. Also shown for comparison are the corresponding results with the cytosol included and with $\mu_l =$ 13.3 μN/m ($\mu_0 = 22.5$ μN/m). The red cell's structural rigidity is observed to be sensitive to variations in in-plane shear modulus of the membrane. A higher shear modulus value indicates the red cell as being more rigid, as can be observed in the reduction in the change in axial diameter. A comparison of columns 1 (simulations with cytosol) and 3 (simulations without cytosol) in Fig. 8 shows that the deformed meshes

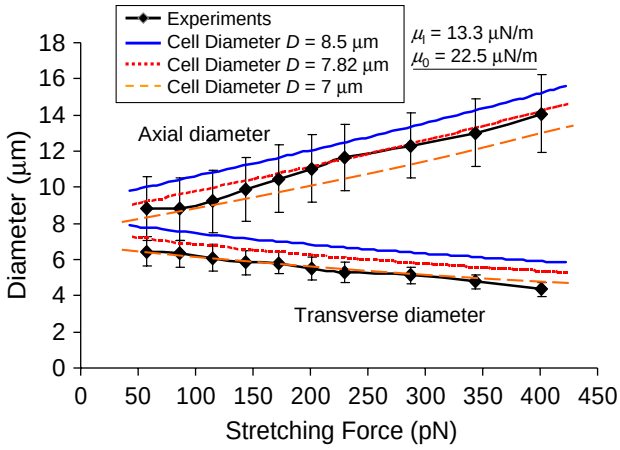

Fig. 9. The predicted effects of varying the cell diameter D from 7, 7.82 to 8.5 μm, respectively. The axial diameter is found rather sensitive to the variations in cell diameter, while the transverse diameter is much less sensitive to the same variations in cell diameter. The result provides an explanation for the much wider scattering in axial response observed experimentally.

modelled with or without cytosol are quite similar, except that the transverse rigidity is considerably increased with the cytosol, consistent with the results plotted in Figs. 5 and 6.

In order to study the effect of the cell size variations, calculations were carried out using three different cell diameters, $D=7.0$, 7.82 and 8.5 μm, respectively. The in-plane shear modulus μ_l was chosen to be 13.3 μN/m (with $\mu_0=22.5$ μN/m) and the contact size d_c was taken to be 2 μm. Fig. 9 shows the predicted effects of varying the cell diameter D from 7 to 8.5 μm. The axial diameter is found to be rather sensitive to the variations in cell diameter, while the transverse diameter is less sensitive to the same variations in cell diameter. The result provides an explanation for the much greater scatter in the experimentally observed changes in axial diameter than in the transverse diameter (see the experimental data and their scatter in both axial and transverse directions in Figs. 6, 7 and 9).

Taking the same set of mechanical properties of the membrane at $\mu_l=13.3$ μN/m (with $\mu_0=22.5$ μN/m), and the same contact diameter at $d_c=2$ μm, Fig. 10 compares the experimental data with the results obtained using the axisymmetric spherical model and the biconcave model, both computed with cytosol. The initial diameter of the spherical cell model was taken to be the same as the biconcave model at 7.82 μm. It is clear that the predicted axial diameter from the spherical model matches very well with that from the biconcave model as well as experiments. However, the spherical model predicts a much stiffer response in the transverse direction as compared to the biconcave model and experiments. Using the spherical model, one can easily match either the axial diameter or the transverse diameter by tuning the shear modulus, but it is not possible to match diameters in both directions well without using the more appropriate biconcave model.

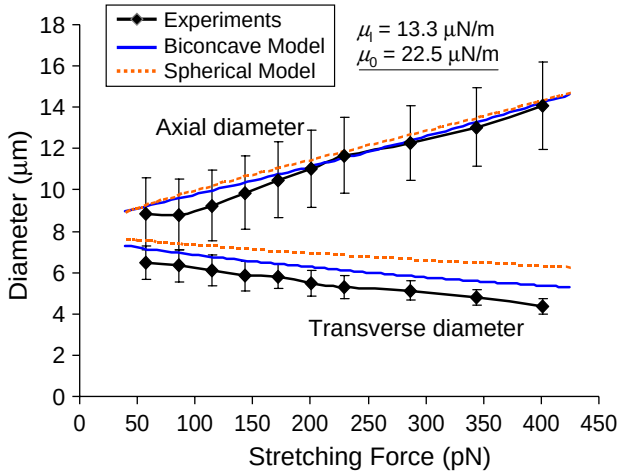

Fig. 10. Comparison of the axisymmetric spherical model and the biconcave model with respect to the experimental results. The predicted axial diameter from the spherical model matches excellently with that from the corresponding biconcave model as well as the experimental curve. However, the spherical model predicted much more stiff response in the transverse direction than the biconcave model when being compared with the experimental results.

Taking the initial cell diameter at 7.82 μm and the shear modulus at $\mu_l = 13.3$ μN/m (with $\mu_0 = 22.5$ μN/m), this average biconcave cell shape has an internal volume of $V_{ave} = 94.1$ μm^3 (Evans and Fung, 1972). Keeping the same membrane shell and filling the internal cell volume with 75%, 100% and 125% of the cytosol V_{ave} (assuming no air), the change in the axial and transverse diameters of the red cell that contain different initial cell interior volumes were computed. The cell interior volume was kept at the initial value during the entire loading process (i.e. no flow of cytosol across membrane during stretching). Fig. 11 shows the predicted effects of varying the cell interior volume while assuming no fluid exchange across the cell membrane. The volume variation is seen to have little effect on the cell's axial response. However, adding or subtracting 25% of the volume of the cell effectively stiffens or softens, respectively, the responses in the transverse diameter under direct uniaxial stretch.

Parametric studies were also performed to consider the experimentally observed scatter in terms of the contact diameter d_c while still keeping the cell size at 7.82 μm and the membrane shear modulus at $\mu_l = 13.3$ μN/m (with $\mu_0 = 22.5$ μN/m). Fig. 12(a) demonstrates that more compliant axial responses and almost identical transverse responses are predicted when the contact diameter decreases from 2 to 1.5 μm and then to 1 μm. The result is again consistent with the much narrower scatter in the transverse response as observed experimentally. Fig. 12(b) shows the range of μ_l and μ_0 values extracted for the present optical tweezers experiments assuming different values, d_c, for the diameter of contact between the beads and the cell membrane. It is clear that while there is a geometrical effect of contact size on the large deformation response, the appropriate range of shear modulus values estimated in Fig. 12(b) is not drastically

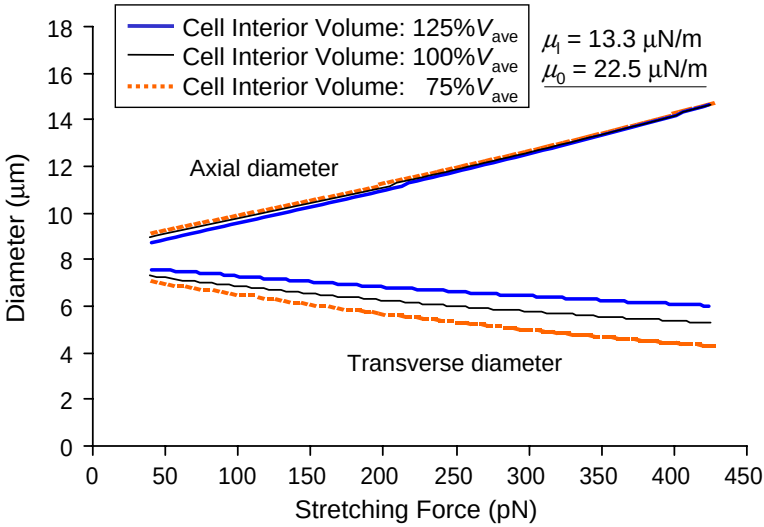

Fig. 11. The predicted effects of varying cell interior volume. The cell interior volume is seen having limited effect on the cell's axial response. However, adding or extracting 25 vol% internal fluid effectively stiffens or softens respectively the transverse rigidity of the cell under direct uniaxial stretch.

altered by the particular choice of d_c. In this respect, we note that prior studies of small deformation of human red blood cells using optical tweezers (Hénon et al., 1999; Sleep et al., 1999; Parker and Winlove, 1999) assumed essentially a point contact between the beads and the cell membrane. It is evident that such an assumption can lead to a more pronounced variation in the shear modulus estimate than that extracted from finite contact diameter simulations which match experiments more closely.

4.2. Effect of the membrane viscosity

When the stretching force imposed by the optical tweezers is released at the point of maximum deformation, the cell returns to its original shape. Using this relaxation response of the cell, the viscoelastic properties of the cell membrane can also be estimated. Adding the viscoelastic term to the constitutive behavior of the cell membrane, Eq. (1) or (4) can be modified as (Evans and Hochmuth, 1976),

$$T_s = T_s^0 + 2\eta \frac{\partial \ln \lambda_1}{\partial t}; \quad t_c = \frac{\eta}{\mu}, \tag{8}$$

where T_s^0 is the membrane shear stress without taking the membrane viscosity into account, and η is the coefficient of surface viscosity of the cell membrane, t is time, and t_c is the characteristic time for relaxation.

When the external stretching force by optical tweezers is released, i.e. $T_s^0 = 0$ in Eq. (8), the characteristic time t_c for the recovery of the red blood cell can be assessed

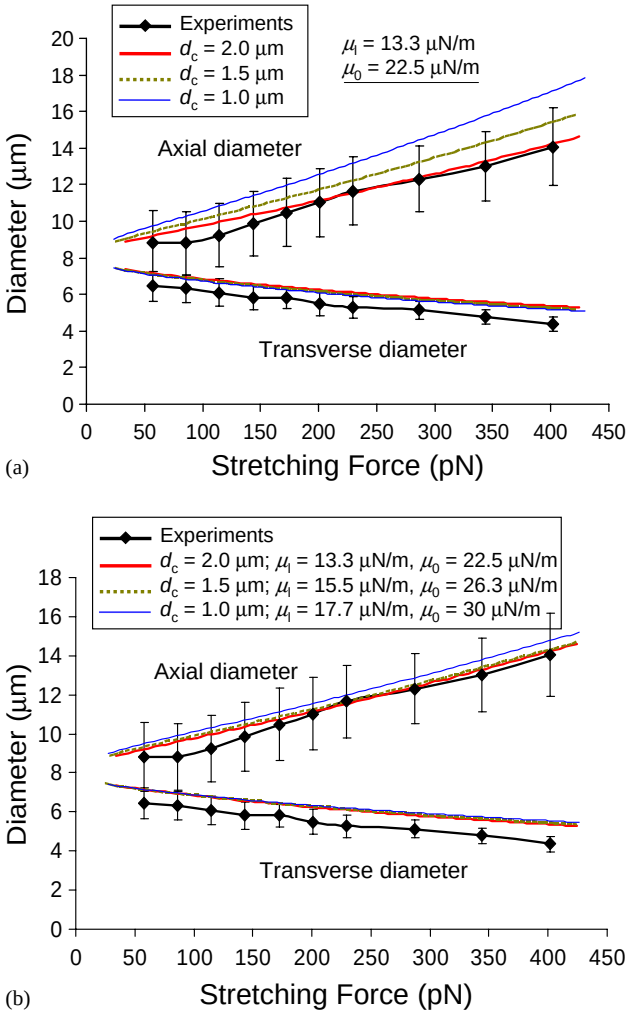

Fig. 12. The predicted effects of varying the contact diameter d_c. (a) More compliant responses are observed when the contact diameter decreases from 2, 1.5 to 1 μm, respectively. (b) The range of μ_l and μ_0 values extracted for the present optical tweezers experiments assuming different values, d_c, for the diameter of contact between the beads and the cell membrane. It is clear that while there is a geometrical effect of contact size on the large deformation response, the appropriate range of shear modulus values estimated is not drastically altered by the particular choice of d_c.

by recourse to the simple expression proposed by Hochmuth et al. (1979):

$$\frac{(\lambda_1^2-1)(\lambda_{1,\max}^2+1)}{(\lambda_1^2+1)(\lambda_{1,\max}^2-1)}=\exp\left(-\frac{t}{t_c}\right), \tag{9}$$

where $\lambda_{1,\max}$ is the initial (maximum) value of the stretch ratio of the red cell. When the best fit to the experimental data on cell relaxation from eight different tests is made

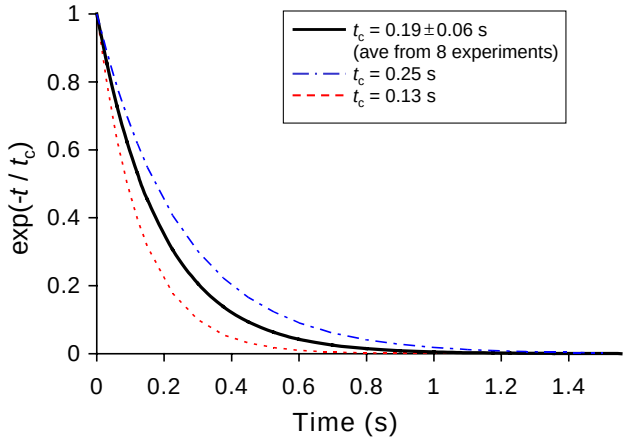

Fig. 13. Best fit to the experimental relaxation data. Using relaxation data from eight different experiments, the characteristic time were estimated to be $t_c = 0.19 \pm 0.06$ s using Eq. (9).

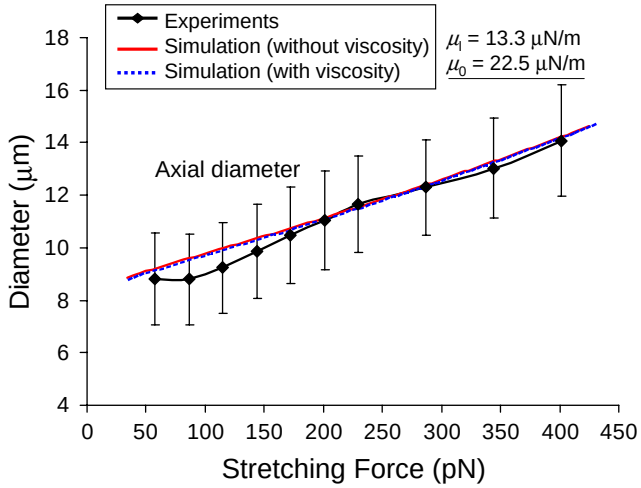

Fig. 14. The effect of the membrane viscosity during loading stage assuming the upper bound values of $t_c = 0.25$ s, $\mu = 22.5$ μN/m in Eq. (8), and a stretch rate $\lambda_1 = 0.3$ s^{-1}.

using Eq. (9), the characteristic time is estimated to be $t_c = 0.19 \pm 0.06$ s. This range of values is slightly higher than the value of $0.1 \sim 0.13$ s estimated from micropipette aspiration experiments (Chien et al., 1978; Hochmuth and Waugh, 1987). The loading response can also be determined by incorporating the viscoelastic term on the right-hand side of the second term of Eq. (8), by recourse to the three-dimensional computational simulation. Figs. 13 and 14 shows a comparison of the predicted changes in axial diameter of the cell as a function of the stretching force, with and without the membrane

viscosity term in Eq. (8). It is evident that the error caused by neglecting membrane viscosity during the loading stage is negligibly small. The transverse diameter change (not shown here) is also not influenced in any significant manner because of the addition of the viscoelastic correction term. Thus the results presented in Figs. 5–12 appear to capture reasonably accurately the overall large deformation loading response of the cell membrane even when the viscoelastic correction factor is ignored.

5. Concluding remarks

We have demonstrated, both in this paper and in our parallel recent work (Lim et al., 2004), that optical tweezers can be used to investigate systematically the large deformation characteristics of the human red blood cell in direct stretch. The present paper provides details of the mechanics of such deformation whereby parametric analyses of the effects of various geometric and material parameters could be examined within the context of loading by means of optical tweezers. The forces through which the deformation is induced in this work are nearly an order of magnitude larger than those achieved previously on red blood cells with optical tweezers (Hénon et al., 1999; Sleep et al., 1999). The method demonstrated here for large deformation testing of living cells provides a potentially powerful new experimental tool, with force capabilities in the range of tens to hundreds of pN, which could complement other techniques such as micropipette aspiration (Evans, 1973; Evans and Skalak, 1980) and atomic force microscopy (Rotsch et al., 1999; Wu et al., 2002). By facilitating direct stretching of a biological cell to large strains in direct tension, the optical tweezers method provides the flexibility to explore the mechanical responses at stress states that are significantly different from those possible with other techniques. In addition, the flexibility of the method to load the cell surface at multiple contact points by the appropriate choice of the number, size and spatial distribution of the beads offers additional capabilities for mechanical testing.

The experimental results obtained for the large deformation of red blood cells in a phosphate buffered saline solution at room temperature have been analysed using a variety of constitutive models and within the framework of a fully three-dimensional computational simulation. An outcome of the exercise is a quantitative assessment of the predictions of different hyperelastic and viscoelastic constitutive formulations on the overall deformation characteristics of the cell subjected to direct tensile stretch by optical tweezers. Also assessed is the characteristic time for relaxation of the red blood cell upon release of the applied force. These results, in conjunction with a wealth of information available in the literature on the deformability of red blood cells probed by other techniques such as micropipette aspiration (see the preceding section), also point to the possible effects of loading mode and stress state on the inferred mechanical response.

The constitutive models used in this study to extract mechanical properties of the cell membrane have been predicated upon continuum analysis. It is clear from the present simulations that, even within the context of continuum analysis, the large deformation response is strongly influenced by a variety of parameters including the loading mode,

contact conditions, geometry and assumed material constitutive characteristics. Recent approaches to analyse large deformation response of red cell membranes (Boey et al., 1998; Discher et al., 1998) have also introduced molecular level models of the deformation of spectrin network in the cell membrane, within the context of Monte Carlo simulations. The results of these simulations were assessed in light of results obtained from micropipette aspiration experiments where the modulus values were found to be consistent with the experimentally extracted values (which were discussed earlier). It should also be recognized that models of cell membrane deformation alone do not capture the dynamic structural changes that evolve in the cell interior. For example, the cytoskeleton could also constitute a structural basis for deformation, mechanical sensing and mechanochemical transduction by providing a mechanical linkage from the extracellular matrix to the cell membrane to the cell interior (e.g., Maniotis et al., 1997).

Ongoing experimental studies (Lim et al., 2003) have also revealed that the present optical tweezers method can be successfully used to identify clearly the connections between red blood cell membrane deformability and the progression of certain types of diseases. In particular, direct stretch experiments involving optical tweezers of normal red blood cells and cells infested in a controlled manner with malaria parasites have revealed quantitative correlations between loss of membrane deformability and exposure to the parasite, at force resolutions on the order of tens of picoNewtons. Such results offer appealing possibilities for further extensions of the present work for diagnostics and drug treatment of diseases.

Acknowledgements

This work was supported by the Nano Biomechanics Laboratory in the Division of Bioengineering at the National University of Singapore, by the Singapore–MIT Alliance, and by the Laboratory for Experimental and Computational Micromechanics at the Massachusetts Institute of Technology.

References

ABAQUS User's Manual, 2002, Version 6.3, ABAQUS Inc., Pawtucket, RI.

Bao, G., Suresh, S., 2003. Cell and molecular mechanics of biological materials. Nature Materials 2 (11), 715–725.

Boal, D., 2002. Mechanics of the Cell. Cambridge University Press, Cambridge, UK.

Boey, S.K., Boal, D.H., Discher, D.E., 1998. Simulations of the erythrocyte cytoskeleton at large deformation. I. Microscopic models. Biophys. J. 75 (3), 1573–1583.

Chien, S., Sung, K.L.P., Skalak, R., Usami, S., Tøzeren, A., 1978. Theoretical and experimental studies on viscoelastic properties of erythrocyte membrane. Biophys. J. 24 (2), 463–487.

Cooke, B.M., Mohandas, N., Coppel, R.L., 2001. The malaria-infected red blood cell: structural and functional changes. Adv. Parasitol. 50, 1–86.

Discher, D.E., Mohandas, N., 1996. Kinematics of red cell aspiration by fluorescence-imaged microdeformation. Biophys. J. 71 (4), 1680–1694.

Discher, D.E., Boal, D.H., Boey, S.K., 1998. Simulations of the erythrocyte cytoskeleton at large deformation. II. Micropipette aspiration. Biophys. J. 75 (3), 1584–1597.

Evans, E.A., 1973. New membrane concept applied to the analysis of fluid shear- and micropipette-deformed red blood cells. Biophys. J. 13 (9), 941–954.

Evans, E.A., 1983. Bending elastic-modulus of red-blood-cell membrane derived from buckling instability in micropipet aspiration tests. Biophys. J. 43 (1), 27–30.

Evans, E.A., Fung, Y.C., 1972. Improved measurements of the erythrocyte geometry. Microvasc. Res. 4, 335–347.

Evans, E.A., Hochmuth, R.M., 1976. Membrane viscoelasticity. Biophys. J. 16 (1), 1–11.

Evans, E.A., Skalak, R., 1980. Mechanics and Thermal Dynamics of Biomembranes. CRC Press, Boca Raton, FL.

Fung, Y.C., 1993. Biomechanics: Mechanical Properties of Living Tissues, 2nd Edition. Springer, New York.

Glenister, F.K., Coppel, R.L., Cowman, A.F., Mohandas, N., Cooke, B.M., 2002. Contribution of parasite proteins to altered mechanical properties of malaria-infected red blood cells. Blood 99 (3), 1060–1063.

Hénon, S., Lenormand, G., Richert, A., Gallet, F., 1999. A new determination of the shear modulus of the human erythrocyte membrane using optical tweezers. Biophys. J. 76 (2), 1145–1151.

Hochmuth, R.M., Waugh, R.E., 1987. Erythrocyte membrane elasticity and viscosity. Ann. Rev. Physiol. 49, 209–219.

Hochmuth, R.M., Mohandas, N., Blackshear, P.L., 1973. Measurement of the elastic modulus for red cell membrane using a fluid mechanical technique. Biophys. J. 13 (8), 747–762.

Hochmuth, R.M., Worthy, P.R., Evans, E.A., 1979. Red cell extensional recovery and the determination of membrane viscosity. Biophys. J. 26 (1), 101–114.

Lenormand, G., Hénon, S., Richert, A., Siméon, S., Gallet, F., 2001. Direct measurement of the area expansion and shear moduli of the human red blood cell membrane skeleton. Biophys. J. 81 (1), 43–56.

Lim, C.T., Dao, M., Suresh, S., Sow, C.H., Chew, K.T., 2004. Large deformation stretching of living cells using laser traps. Acta Materialia, in press.

Lim, C.T., Lee, Y.S., Tan, K., Dao, M., Suresh, S., 2003. Unpublished research. National University of Singapore and Massachusetts Institute of Technology.

Maniotis, A.J., Chen, C.S., Ingber, D.E., 1997. Demonstration of mechanical connections between integrins, cytoskeletal filaments, and nucleoplasm that stabilize nuclear structure. Proc. Natl. Acad. Sci. USA 94 (3), 849–854.

Parker, K.H., Winlove, C.P., 1999. The deformation of spherical vesicles with permeable, constant-area membrane: applications to the red blood cell. Biophys. J. 77 (6), 3096–3107.

Platt, O.S., 1995. The sickle syndrome. In: Haldin, R.I., Lux, S.E., Stossel, T.P. (Eds.), Blood: Principles and Practice of Hematology. J. B. Lippincott, Philadelphia, pp. 1592–1700.

Rotsch, C., Jacobson, K., Radmacher, M., 1999. Dimensional and mechanical dynamics of active and stable edges in motile fibroblasts investigated by using atomic force microscopy. Proc. Natl. Acad. Sci. USA 96 (3), 921–926.

Sheetz, M.P., 1998. Laser Tweezers in Cell Biology. Academic Press, London, UK.

Simo, J.C., Pister, K.S., 1984. Remarks on rate constitutive equations for finite deformation problems: computational implications. Computer Methods in Applied Mechanics and Engineering 46 (2), 201–215.

Sleep, J., Wilson, D., Simmons, R., Gratzer, W., 1999. Elasticity of the red cell membrane and its relation to hemolytic disorders: an optical tweezers study. Biophys. J. 77 (6), 3085–3095.

Wu, T., Lee, G.Y.Y., Phan-Thien, N., Lim, C.T., 2002. Investigating the mechanical properties of human platelets and erythrocytes using atomic force microscopy. International Congress on Biological and Medical Engineering, Singapore.

Van Vliet, K.J., Bao, G., Suresh, S., 2003. Experimental mechanics techniques for living cells and biomolecules. Acta Materialia 51 (19), 5881–5905.